IEEE Access
Multidisciplinary | Rapid Review | Open Access Journal

Received 27 November 2023, accepted 18 December 2023, date of publication 29 December 2023,
date of current version 22 January 2024.

Digital Object Identifier 10.1109/ACCESS.2023.3348145

RESEARCH ARTICLE

Intelligent Control Method Research for High Rise Building Vibration by Integrating Genetic Algorithm and LSTM

JIJUN ZHANG AND YANMIN XUE
School of Art and Design, Xi'an University of Technology, Xi'an 710054, China
Corresponding author: Jijun Zhang (techfuturezhang@163.com)

This work was supported by the 2017 Ministry of Education Planning Fund of Humanities and Social Sciences under Grant 17YJAZH100.

ABSTRACT In order to solve the problem of performance degradation, such as local optimality, that may occur when shallow learning is used to predict the high-rise buildings seismic response under difficult conditions, a high-rise building vibration intelligent control method integrating genetic algorithms and long short-term memory networks is proposed. First, a structural response prediction model is constructed and combined with vibration control theory. Furthermore, an intelligent control algorithm using long short-term memory networks is designed. In conjunction with this algorithm, a centralized controller that integrates convolutional neural networks at different levels is designed. The structure of the centralized control system is improved, and genetic algorithms and Lyapunov stability theory are used to optimize thenetwork hyperparameters through deep learning. The results showed that this framework had high prediction accuracy, with the smallest relative difference in predicting C-library data at -0.0053 cm on average. The largest prediction error for B-library data was 0.015 cm on average. The long short-term memory network had the smallest prediction error and the best learning and prediction performance. When the degradation level of each layer stiffness in the benchmark model was between 10.2% and 20.5%, this intelligent controller achieved the best control effect, maintaining above 39.8%. Optimized using genetic algorithm, the optimal fitness value after 80 iterations represented controllerloss function value, which were 8.3×10.5, 2.3×10.4, 2.2×10.4, and 3.0×10.4, respectively, demonstrating good prediction results. Compared with traditional trial calculation methods, this algorithm has higher computational efficiency and accuracy. The fusion of genetic algorithms and long short-term memory networks with different structural forms shows good seismic reduction effects on the time responses of benchmark models. The research method has good prediction accuracy, high reliability, and flexible system design, providing new strategies for intelligent control of high-rise building structures under different conditions.

INDEX TERMS Genetic algorithm, LSTM, architecture, structure, intelligent control.

I. INTRODUCTION

It is necessary to apply direct or indirect vibration control measures to buildings to minimize the negative impact of earthquakes on human society [1]. With the rapid increase in population density and the shortage of land resources, people are gradually exploring higher height and larger span building structural forms. In recent years, many domestic and foreign research institutions have made significant breakthroughs in structural vibration control, forming a series of new control theories and methods. However, for complex high-rise buildings, the control effect may not be satisfactory [2]. Due to the instability of energy input and high system costs, traditional control technologies are still under in-depth research and have relatively few applications in engineering [3]. Intelligent control combines the advantages of traditional control and artificial intelligence, with a wider range of applications and control effects that are more in line with practical

The associate editor coordinating the review of this manuscript and approving it for publication was Min Wang.

engineering [4]. In addition, intelligent control can also be combined with traditional control algorithms and other intelligent control algorithms, utilizing the different advantages of the two to achieve the best control effect. In intelligent algorithms, genetic algorithms are applied to the optimal placement of actuators and the linear quadratic regulator (LQR) algorithm with discrete-time state feedback, which is much better than traditional LQR active vibration control [5]. Regarding the issue of control performance, artificial intelligence theory has a wide range, and deep learning is a new direction of artificial intelligence, with a focus on improving the model depth of the network and the learning accuracy of feature extraction. Currently, mature research frameworks include Long Short Term Memory (LSTM), Convolutional Neural Networks (CNN), and others.

In this study, a new intelligent control algorithm is proposed by combining LSTM with structural vibration control theory. Using the 20-layer Benchmark model as the control object, the CNN-LSTM centralized controller with 1 and 2 dimensions is proposed for vibration control of the structure. According to Lyapunov theory, GA-LSTM intelligent decentralized controller is constructed by using GA to optimize controller hyperparameters. The research aims to achieve the goal of reducing the degree of building damage by scientifically and reasonably predicting and controlling the vibration response of high-rise building structures during earthquakes, and also provide new ideas for the seismic theory and technical application of building structures.

The research mainly includes five parts, and in the first part of the article, the background and significance of research on intelligent vibration control are mainly introduced. The content of Part 2 is a summary of the intelligent control technology for building vibration. The third part is the research method content, mainly divided into two sections. In section I, a structural intelligent control algorithm based on LSTM is proposed. In section II, the study integrates CNN hierarchical feature learning to improve the LSTM centralized controller. Based on Lyapunov theory, the sufficient condition of stability of the sub-controller is deduced, and the hyperparameters of the sub-controller are optimized by genetic algorithm. A decentralized control model of high-rise building structure vibration response based on GA-LSTM optimization algorithm is constructed.The fourth part is about verifying the effectiveness of the research model. The fifth part is a summary of the most research methods and an analysis of the experimental results. At the same time, the shortcomings of research methods and future research directions are proposed.

II. RELATED WORKS

Currently, intelligent control of building structures has a wider range of adaptability and practical engineering control effects, and the implementation of equipment systems is simpler, making it a hot field of control research. Hamza A et al. proposed an intelligent control method using artificial neural networks to obtain an active suspension system, and provided information about the system through physical laws to determine system parameters. The results showed that this method had good performance in graphical and simulation output validation [6]. Song Y's team designed asolution for high-rise buildings vibration suppression. They mainly developed a high-rise building structures model through the Hamiltonian principle, and used the Lyapunov direct method to make the closed-loop system uniformly bounded in the time domain. The results showed that the designed method was effective [7]. Ma et al. proposed a numerical model to predict the vibration of buildings caused by subway trains operating in curved tunnels, and established corresponding models to predict the vibration of buildings. The results indicated that the model provided a track solution for implementing vibration control [8]. Konar and Ghosh and other scholars designed a shallow liquid level that remained constant between the free liquid level and the floating base to overcome the basic shaking frequency changes caused by liquid level fluctuations in the tank. The results showed that in an example building's water storage tank system, a reduction in structural response was achieved [9].

Structural vibration is mainly caused by ground motion excitation, and its structural safety is the main goal of building technology development. To achieve this goal, Fali et al. proposed a passive control strategy in which no energy was required to ensure the reduction of structural vibration caused by ground motion excitation. The results verified the effectiveness of this method [10]. Control algorithms are the most critical aspect for successfully controlling civil structures under earthquake and wind effects. Adaptive intelligent control algorithms have gradually become an acceptable alternative method. Saeed M U's team made the practical application of vibration response attenuation of intelligent civil structures possible from the perspective of artificial intelligence to create an intelligent civil structure. The results showed that this method had obvious technical advantages [11]. Active vibration control systems are usually considered the most effective method for structural vibration control, but the type of ground motion may greatly affect their performance. To solve it, Elias et al. designed a linear quadratic Gaussian control algorithm that considered the situation under earthquakes and incorporated the nonlinear behavior of the structure into seismic analysis. The results showed that this method improved model robustness [12]. To cope with the vibration and structural damage of super high-rise buildings by natural disasters, Gao et al. established a new finite dimensional dynamic model using the assumed mode method. The results verified the effectiveness of this method in vibration suppression [13].

In summary, for complex buildings, the control effect may not be satisfactory. Active control technology is still in the further research stage due to the main issues of unstable energy input and high system cost, and its engineering applications are relatively limited.Intelligent control is a new type of theory with highly interdisciplinary properties. Compared to traditional control theory, intelligent control has the

advantages of rapid response, large force, and low energy consumption. Deep learning has many advantages compared to shallow learning. Combining it with vibration control theory and applying it to intelligent buildings vibration control is a relatively novel and practical work.To reduce the vibration response of structures during earthquakes and achieve the goal of reducing the degree of building damage, this study proposes an intelligent control method for high-rise building vibration that integrates genetic algorithm and short-term memory network.

III. DESIGN OF INTELLIGENT VIBRATION CONTROL MODEL FOR TALL BUILDING STRUCTURES BASED ON GENETIC ALGORITHM AND LSTM NETWORK

Buildings can experience complex structural responses with significant and random variations under various external factors such as earthquakes and typhoons. In active intelligent control algorithms, a large amount of structural response information is required to command actuators in order to control structural vibration. In order to extract and improve the intrinsic relationships within nonlinear data and obtain structural responses, a structural response prediction model is first constructed and combined with vibration control theory. Furthermore, an intelligent control algorithm based on LSTM is designed. In conjunction with this algorithm, a centralized controller that integrates CNN at different levels is designed. The structure of the centralized control system is improved, and genetic algorithms and Lyapunov stability theory can optimize the hyperparameters of LSTM network through deep learning. Ultimately, a distributed control model for high-rise building structural vibration response based on GA-LSTM optimization algorithm is developed.

A. STRUCTURAL RESPONSE PREDICTION METHOD BASED ON LSTM

LSTM has added a state c on top of the original RNN to address its sensitivity to short-term inputs [14]. Without changing the training algorithm, LSTM can effectively extend memory time and improve its reliability. The general formula for the accumulation of structural errors in LSTM networks at any time is shown in equation (1).

$$\delta_k^T = \delta_{f,j}^T W_{fh} + \delta_{i,j}^T W_{ih} + \delta_{\tilde{c},j}^T W_{ch} + \prod_{j=k}^{t-1} \delta_{o,j}^T W_{oh} \quad (1)$$

Reply: Thank you very much for your valuable advice, and the unnecessary basics in the method have been cut. Please review. Thank you. f represents the forgetting gate, $\tilde{c}$ represents the corrected state storage unit, and o represents the corrected output gate output. $\delta_{f,j}^T$, $\delta_{i,j}^T$, $\delta_{\tilde{c},j}^T$, $\delta_{o,j}^T$ represent the error at time t of each link. W_{oh} represents the weight matrix. During data training, over-fitting is the main problem with shallow learning, which manifests as a decrease in the generalization performance of the network model. Comparing the LSTM training process to the process of information transmission, the criteria for over-fitting are shown in equation (2).

$$|\Delta W| \cdot |\Delta Y| \geq \frac{TPh}{2\log_2(1+M/N)} \quad (2)$$

In equation (2), T represents the correlation function, and h represents the number of network nodes. M represents the normalized output value, P represents the over-fitting parameter, and N represents the root mean square error. ΔW represents the weight variable ratio trained twice for LSTM over-fitting, and $N \approx \Delta Y$ represents the prediction error. When there is over-fitting in LSTM, $N \approx \Delta Y$, as shown in equation (3).

$$p \leq \frac{2|\Delta W| \cdot |\Delta Y| \cdot \log_2(1+M/N)}{Th} \quad (3)$$

In equation (3), the smaller the value of p, the less over-fitting occurs during network operation. If p decreases first and then increases, it indicates over-fitting in network training. In the LSTM network structure, methods that can effectively solve over-fitting include weighted parameter regularization, Dropout technology, and so on. Regularization is to reduce the complexity and generalization error of deep learning models by adding constraints to the loss function. The calculation expression is shown in equation (4).

$$\tilde{J}(w^{\cdot}, x, y) = J(w^{\cdot}, x, y) + \alpha\Delta(w) \quad (4)$$

In equation (4), $\tilde{J}$ represents the regularized loss function, and J represents the loss function. $\Delta(w)$ represents the contribution coefficient, and α represents the constraint term. Research using L_2 regularization, i.e. $\Delta(w) = \|w\|_2^2$. In the LSTM deep learning model, the Dropout technique is introduced to prevent over-fitting. Dropout technology modifies the structure of LSTM networks, resulting in random failure of the weight matrix of hidden layer neuron nodes. The working principle of Dropout technology is shown in Figure 1 (a). The robustness of connections between hidden layer random subset nodes is improved while reducing network consensus. Equation (5) is the mathematical expression for the LSTM layer after using Dropout technology.

$$\begin{cases} r_i^{(l)} \sim Bernoulli(p') \\ \tilde{x}^{(l)} = r^{(l)} \times x^{(l)} \\ z_i^{(l+1)} = w_i^{(l+1)} \tilde{x}^{(l)} + b_i^{(l+1)} \\ y_i^{(l+1)} = f\left(z_i^{(l+1)}\right) \end{cases} \quad (5)$$

In equation (5), $r_i^{(l)}$ represents the j-th Dropout strength coefficient of layer l. p' represents the Bernoulli distribution probability. $x^{(l)}$, $\tilde{x}^{(l)}$ represent the input value of layer l and the corrected input value, respectively. $w_i^{(l+1)}$ represents the i-th weight coefficient of the $l+1$-th layer. $b_i^{(l+1)}$ represents the i-th deviation value of the $l+1$-th layer. $z_i^{(l+1)}$ represents the i-th output value of the $l+1$-th layer. $l+1$ represents the activation function, and $y_i^{(l+1)}$ represents the output value of the i-th activated layer in layer $l+1$. Early stopping

technology is a method of adaptively selecting Epoch values, used to calculate the training error of each Mini batch segment and compare it with the results of the previous period. The working principle of Early Stopping technology is shown in Figure 1 (b).

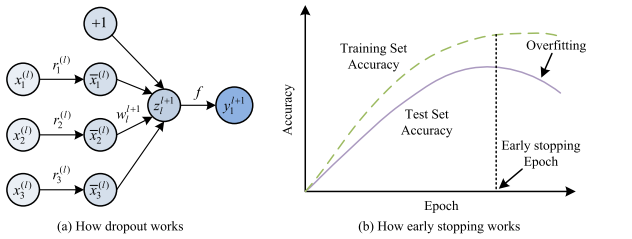

FIGURE 1. The working principle of dropout technology and early stopping technology.

When there are too few hyperparameters Epoch in the model, the data training effect is poor, leading to underfitting. When there are too many hyperparameters in the model, the over-fitting probability will increase due to the increase of noisy data. Early stopping technology can truncate Epoch as the error increases, and use the minimum error iteration value corresponding to Epoch as the final network hyperparameter. If $L(t)$ is defined as the training proportion loss of Early Stopping technology, then there is equation (6).

$$L(t) = 100 \cdot \left[\frac{E_{test}(t)}{E_m(t)} - 1 \right] \% \tag{6}$$

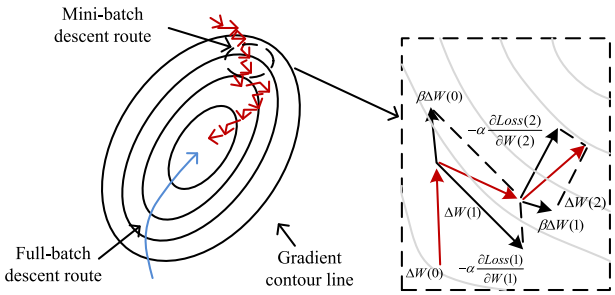

FIGURE 2. Gradient descent paths of different algorithms.

In equation (6), $E_{test}(t)$ represents the test error. $E_m(t)$ represents the optimal testing error for network training to time t. In the LSTM network structure, methods that can effectively solve local optimal problems include adaptive learning rate α, Mini-batch random gradient descent, etc. [15]. The LSTM control algorithm proposed in the study is the Adam algorithm, which can make reasonable changes to the learning rate in situations with high gradient coefficients and noise. As shown in Figure 2, there are gradient descent paths for different algorithms.

In Figure 2, in a Full batch, an epoch only contains one iteration step. The Mini-batch random gradient descent divides the database into multiple batches. At the same time, it quantifies the data of each batch and updates the parameters. The calculation expression of the variation of the weight matrix with step size is shown in equation (7) [16].

$$\Delta W(t) = \beta \Delta W(t-1) - \alpha \frac{\partial Loss(t)}{\partial W(t)} \tag{7}$$

In equation (7), α represents momentum and β represents exponential decay rate. The tanh function is used as the activation function for LSTM gate operations and the Relu function as the activation function for the state and final output of LSTM units. Due to the fact that the data distribution of deep learning has the same conditional probability but no edge probability, Zhejiang has led to excessive changes in deep unit nodes distribution. Thus, normalization techniques are used in LSTM. The displacement data generated by vibration in building structures have weak boundary sense and strong disorder. Therefore, for the processing of input data, the Z-score normalization method is more suitable. Considering the variation pattern of building displacement values caused by vibration and the length of the database itself, four hidden layers were selected. The output layer is a linear regression layer, and its number of nodes is determined by the hidden layer construction of the LSTM depth framework. The output content is the displacement response at the time. The object of predicting building vibration response is the displacement of building structures at different times, which is a nonlinear regression problem based on time series. When constructing a deep learning framework for it, the mean square error of all data will be used as the objective function. By combining the over-fitting scheme, equation (8) can be obtained.

$$Loss = MSE(y_t, y_t) = \frac{1}{N} \sum_{t=1}^{N} \left(y_t - \widetilde{y_t} \right) + \alpha \left\| w \right\|_2^2 \tag{8}$$

In equation (8), N counts databases. $y_t, \widetilde{y_t}$ represent the displacement calculation and predicted values at each time. The value of α is 0.04. The smaller the objective function value, the better the learning and prediction performance of LSTM prediction on the data. Based on the LSTM based structural response prediction model proposed above, a 3-layer Benchmark framework structure is used as an example model. The damping ratios of the first and second modes are all 0.05, using Rayleigh damping, with actuators arranged on all three layers. The system motion equation is shown in equation (9).

$$KX(t) + M\ddot{X}(t) + C\dot{X}(t) = B_s U(t) - m\ddot{x}_g(t) \tag{9}$$

In equation (9), B_s represents the position matrix. C, K, M represent the damping matrix, stiffness, and mass, respectively. The formula for converting space is shown in equation (10) [17].

$$\dot{Z}(t) = AZ(t) + BU(t) + D\ddot{X}_g(t) \tag{10}$$

In equation (10), X represents seismic acceleration, $U(t)$ represents control force vector, and $Z(t)$ represents system state vector. Based on the motion equation and spatial equation of the building structure, a Simulink simulation

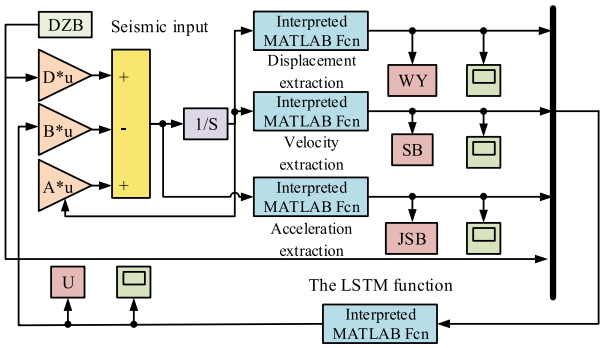

FIGURE 3. Simulink simulation system based on LSTM.

system for the LSTM controller can be established, as shown in Figure 3.

In Figure 3, the core of the simulation system is a deep learning framework based on LSTM. Obtained by adjusting the LSTM structural response prediction model. Embed the LSTM controller into the intelligent control simulation model of this structure in the form of writing an S function. The input of this system is seismic acceleration, and the LSTM controller is used to collect the response feedback of the control force applied to the building structure. Thus achieving the goal of real-time reduction of structural response. The Linear Quadratic Regulator (LQR) algorithm for discrete-time state feedback has a high requirement for the accuracy of the structural model, but its structure is simple and easy to implement. Therefore, the study adopts this algorithm to collect calculation data. Apply a 30s El-centrowave to the structure and set the frequency to 0.02 s/time. Normalize and train the input LSTM control data, with the same objective function as equation (8).

B. DECENTRALIZED CONTROL MODEL FOR VIBRATION RESPONSE OF TALL BUILDING STRUCTURES BASED ON GENETIC ALGORITHM AND CNN-LSTM OPTIMIZATION ALGORITHM

For highly complex inductive problems, extracting complex function expressions that describe the laws of the problem is the key. The currently widely used and effective method is neural network algorithm, among which the most classic algorithms include Back Propagation (BP), Radial Basis Function (RBF), CNN, etc. [18]. CNN can perform good data feature extraction for one-dimensional, two-dimensional, and three-dimensional information. As shown in Figure 4, it is a three-dimensional CNN framework diagram [19].

In Figure 4, the convolutional layer of CNN contains several sets of parameters, which are called several convolutional kernels. Each filter can convolution the raw data to obtain a feature map, which is called a channel. The elements of the feature map are shown in equation (11) [20].

$$a_{i,j} = f\left(\sum_{d=0}^{D-1}\sum_{m=0}^{F-1}\sum_{n=0}^{F-1}\omega_{d,m,n}x_{d,i+m,j+n} + \omega_b\right) \tag{11}$$

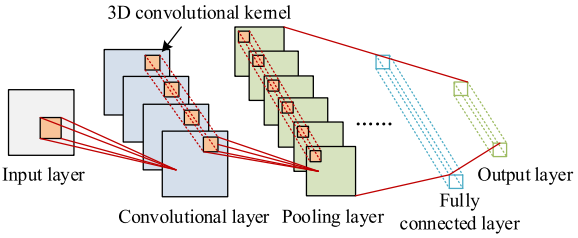

FIGURE 4. 3D-CNN frame.

In equation (11), $f(\cdot)$ represents the activation function, using the Relu function. D represents the filter depth, and F represents the convolutional kernel size. represents the weights of m rows and n columns in the d layer of the convolutional kernel. ω_b is the bias term of the convolutional kernel, and $x_{d,i+m,j+n}$ is the d-layer m-row n-column graph element. Assuming the dimension of the input data is $n \times n$, the step size is set to s, and the number of fills is p. After convolution calculation, the output data dimension is shown in equation (12).

$$\left[\frac{(n+2p-F)}{s}+1\right] \times \left[\frac{(n+2p-F)}{s}\right] \tag{12}$$

The feature extraction method of CNN directly affects the calculation of errors in convolution and pooling layers. There are no parameters that need to be learned in the downsampling operation of the pooling layer, therefore, it only plays a role in error backpropagation during the training process of the pooling layer, and there is no calculation of weight gradients. Maximizing pooling will transfer the error term of this layer unchanged to the neuron where the maximum value of the corresponding region is located in the previous layer, while the error values of other neurons are all 0. Similarly, average pooling distributes the error term of this layer evenly to all neurons in the corresponding region of the previous layer. To quantitatively study the working logic of CNN operation, the DeepDream visual algorithm and AugmentedImageDatastore function were used to extract and analyze local features of each channel and complete features of each network layer in the network [21]. The specific expression of the DeepDream visual algorithm is shown in equation (13) [22].

$$I = \text{DeepDreamImage}(net, layer, chamnnels, name, value) \tag{13}$$

In equation (13), *layer* represents the hidden layer for extracting visual features. *net* represents the pre trained network structure. *chamnnels* represents the vector of the channel index. *value*, *name* represent the parameter values and names of the input data, respectively. The AugmentedImageDatastore function can be used to automatically resize features, but it must be used in conjunction with the Activations function to extract the complete features of the designated network layer. The expression of this function is

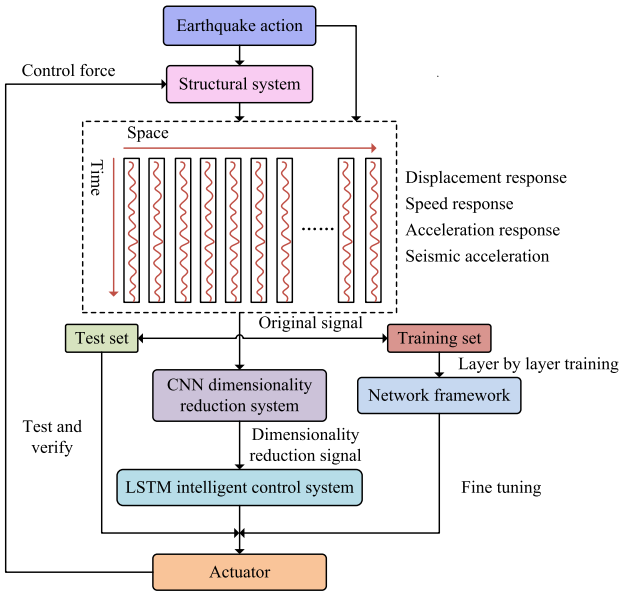

FIGURE 5. Control simulation flow of CNN-LSTM centralized controller.

shown in equation (14)

$$\begin{cases} auimds = Augmented\text{ImageDatastore}\,(outputsize, imds) \\ features = Activations\,(net, caugimds, layer) \end{cases} \tag{14}$$

In equation (14), *outputsize* represents the output size, and *imds* represents the dataset. *auimds* represents the batch processed dataset. Figure 5 shows the control simulation process using the CNN-LSTM centralized controller.

In Figure 5, the data input to the CNN dimensionality reduction system is theacceleration response, velocity, displacement, and seismic acceleration of the 20-layer Benchmark model under seismic excitation, totaling 61 dimensions. The first two-thirds data is used as training data, and the remaining is used as test data. After dimensionality reductionprocessing on convolutional kernels of different sizes, they are then fed into the LSTM intelligent control system to generate actuator control forces. Simultaneously applied to the Benchmark model to quickly collect, analyze, and control vibration of data. At present, the most widely used centralized control strategy has exposed many drawbacks, and decentralized control strategies based on large system theory have therefore received widespread attention. However, this strategy has not yet been widely adopted in the field of civil engineering. The research focuses on high-rise civil engineering structures under earthquake action, and improves the structures of several control systems. Assuming that the actuators of the controlled K-story high-rise building structure are fully distributed and dispersed into N subsystems, and there is no overlap between each subsystem. The i subsystem contains k floors. Displacement vector X_i and control force vector U_i are shown in equation (15) [23].

$$\begin{cases} X_i = \left[x_j, \ldots, x_{j+k}\right]^T_{k\times 1} \\ U_i = \left[u_j, \ldots, u_{j+k}\right]^T_{k\times 1} \end{cases} \tag{15}$$

The state space equation is shown in equation (16).

$$\dot{Z}_i = A_i Z_i + B_i U_i + E_i \ddot{x}_g + \sum_{j\neq i} A_{ij} Z_j + \sum_{j\neq i} B_{ij} U_j \tag{16}$$

The main computational blocks of the LSTM sub controller include forward core algorithms, error backpropagation, and optimizing the processor. If it is set as the input at time t of the substructure LSTM controller, then there exists equation (17).

$$P_{j,t} = \left[X_{i,t}\ \dot{X}_{i,t}\ \ddot{X}_{i,t}\ a\right]^T_{(3k+1)} \tag{17}$$

In equation (19), a represents seismic acceleration. $X_{i,t}$ represents the output of the j controller at t. By combining equations (15) and (16), complete dispersion and overlapping dispersion control equations can be obtained, as shown in equation (18).

$$\begin{cases} h_{j,t} = U_{j,t} \\ h_{j,t} = \bar{U}_{j,t} \end{cases} \tag{18}$$

The LSTM sub controller adopts the Backpropagation Through Time (BPTT) algorithm for error backpropagation [24]. Firstly, the input values of the LSTM sub controller are calculated at each moment, and time and network levelsare used as the backpropagation directions respectively. Then the errors of each LSTM unit are calculated using the formula, and then the weights of each unit in the LSTM hidden layer are calculated. Finally, the unit weights are updated using the optimization processor Adam. As shown in Figure 6, it is the schematic diagram of the LSTM decentralized control system.

Based on Lyapunov stability theory, LSTM sub-controllers stability is studied and sufficient conditions to be stable are derived. Controller output error is set as shown in equation (19).

$$E\,(t) = y\,(t) - \hat{y}\,(t) = \Delta y\,(t) \tag{19}$$

In equation (19), $y\,(t)$ represents controller's actual output value. $\hat{y}\,(t)$ is the predicted output value of LSTM. Error energy function is shown in equation (20).

$$\zeta\,(t) = \frac{E^2\,(t)}{2} \tag{20}$$

The neuron activation function is derived at a sufficiently high sampling frequency, as shown in equation (21).

$$\sigma'\,(t) = \frac{\Delta y\,(t)}{\Delta u\,(t)}\,|_{\Delta t\to o} = \frac{dy\,(t)}{du\,(t)} \tag{21}$$

In equation (21), $u\,(t)$ represents controller input value, and W represents weight coefficient matrix. The BPTT algorithm is used for error backpropagation, and the formula

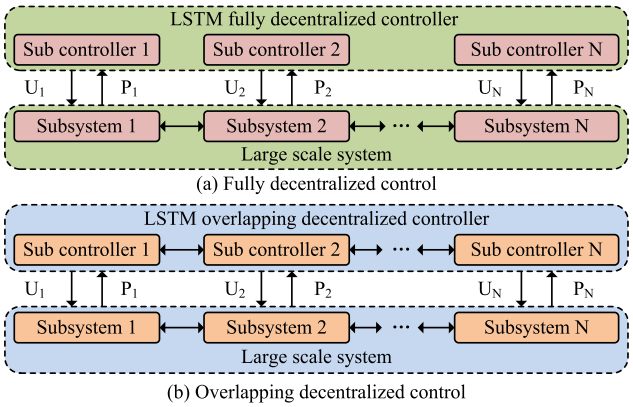

FIGURE 6. Schematic diagram of LSTM decentralized control system.

for updating the LSTM weight coefficient matrix is shown in equation (22).

$$\Delta w_{ji}(t) = \alpha E(t)\,\sigma'(t)\,h_i(t-1)\,\frac{\partial u(t)}{\partial net_j(t)} \tag{22}$$

In equation (22), $\Delta w_{ji}(t)$ counts the change from the i to j. The initial learning rate α also has a significant impact on LSTM sub-controller stability. In LSTM, α controls the adjustment speed. When F is too small, the rate of loss gradient decrease and the convergence time is longer. When α is too large, the descent process may cross the optimal value and obtain a suboptimal value. Therefore, it is necessary to optimize α. Genetic algorithms can establish an initial population set of parameters to be optimized and eliminate inferior individuals based on fitness functions. Screen out the best offspring and continuously update the population set to obtain the optimal solution [25]. A new parameter optimization method was proposed by combining genetic algorithm, as shown in Figure 7.

In Figure 7, for the initial learning rate optimization problem of GA-LSTM sub controller, the fitness function adopts the loss function of the LSTM deep learning framework. The construction of the GA-LSTM deep learning prediction framework uses El-centro waves with wider motion frequency bands. The adoption period is set to 0.02 seconds and the time positioning is calculated for 30 seconds. The training data is the first 1000 sets of data calculated by the LQR control algorithm, and the data is normalized before training. The control forces of each layer at the previous moment are used as the output of the prediction framework. After building the framework, it is compiled into Simulink to complete the design of the GA-LSTM intelligent decentralized controller. After inputting unknown structural responses and seismic acceleration data into the controller, suitable real-time control forces can be predicted. The network structure for centralized control is 61 × 300 × 20, including condition 1, 2, 3, and 4. The schematic diagram of each working condition is shown in Figure 8.

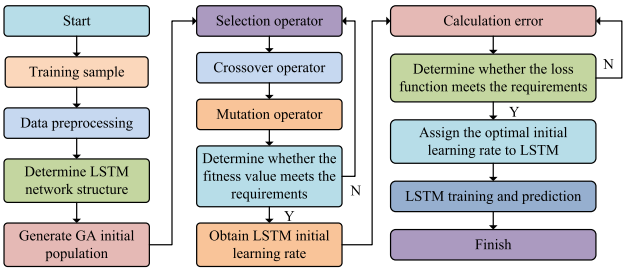

FIGURE 7. GA-LSTM hyperparameter optimization flow chart.

In Figure 8, n_i represents the numbering of each subsystem. Condition 1 and Condition 2 are used to investigate the influence of the number of subsystems on control effectiveness. Overlapping decentralized in a chain topology - 5 subsystems (Condition 3) are compared with Conditions 1 and 2 to study the effect of controller overlap. Overlapping decentralized in a chain topology - 6 subsystems (Condition 4) are compared with Conditions 2 and 3 to study the influence of the number of overlapping controllers. A comparison is made with LQR centralized control (Condition 5). The number of LSTM layer units is determined by a combination of experience and trial calculations, aiming to minimize the loss function of the prediction framework and optimize the output effectiveness of the controller's control force. It is assumed that the control force applied to the overlapping region is opposite to the direction of structural vibration, and the control force output for adjacent subsystems with overlapping actuators is defined as shown in equation (23).

$$\overline{u_k} = \begin{cases} -\nabla\left(u_{j,k}, u_{j-1,k'}\right) \cdot \dfrac{1}{2}\left(\left|u_{j,k}\right| + \left|u_{j-1,k'}\right|\right), \\ \qquad \left(u_{j,k} \cdot u_{j-1,k'} \geq 0\right) \\ -\mathrm{sgn}\left(u_{j,k} \cdot x_j\right) \cdot \max\left(\left|u_{j,k}\right|, \left|u_{j-1,k'}\right|\right), \\ \qquad \left(u_{j,k} \cdot u_{j-1,k'} < 0\right) \end{cases} \tag{23}$$

In equation (23), sgn $(\cdot)$ represents the symbolic function. $u_{j,k}$ is actuatorcontrol forcewith subsystem j number k. The calculation expression of $\nabla(\cdot)$ is shown in equation (24).

$$\nabla(\cdot) = \begin{cases} \mathrm{sgn}\left(u_{j-1,k'}\right), & \left(\left|u_{j,k}\right| \geq \left|u_{j-1,k'}\right|\right) \\ \mathrm{sgn}\left(u_{j-1,k'}\right), & \left(\left|u_{j,k}\right| < \left|u_{j-1,k'}\right|\right) \end{cases} \tag{24}$$

IV. EXPERIMENTAL RESULTS ANALYSIS OF THE EFFECTIVENESS OF INTELLIGENT VIBRATION CONTROL MODEL FOR HIGH-RISE BUILDINGS

In the finite element software Abaqus 6.13, a steel cantilever beam model was established using beam elements. The structural dimensions were 2.5 × 0.3 × 0.2 m, with a density mainly of 7800 kg/m3. The elastic modulus was taken as 2.06 × 105 MPa, and the Poisson's ratio was set to 0.3. A concentrated vertical downward stress of 1 kN was applied at the cantilever end. The fixed end was restrained, with a mass of 9.36 × 104 kN applied, and seismic wave excitation was applied in the long side direction of the fixed end of the cantilever beam. Three different seismic waves

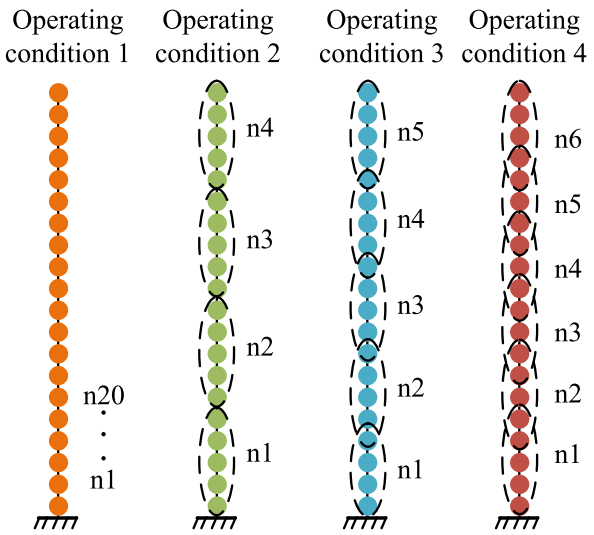

FIGURE 8. Schematic diagram of each working condition.

with distinct data characteristics were selected as input excitation: E1-centro wave, Ninghe Tianjin wave, and artificially synthesized wave. Displacement values were chosen as the predicted quantities, and the displacement values at the breakpoint of the beam cantilever were calculated, serving as three displacement databases, as shown in Table 1.

In Table 1, displacement value data from Library A were selected for framework construction, and the network architecture was trained with 1-800 sets of data. A library 801-1500 sets of data, B and C libraries were used to test the network architecture constructed. The 20-layer Benchmark model designed by ASCE was selected as the simulation example. Assuming that the horizontal stiffness of the floor is infinite, the static condensation method is used to reduce the order of the original finite element model, only 20 translational degrees of freedom are retained, and each layer of the actuator is fully distributed. The structure parameters of Benchmark after condensation are shown in Table 2 [26].

The LSTM deep learning framework used an Adam optimizer with four gate operations, and the output activation function used tanh and relu functions to set the initial learning rate to 0.008. As shown in Figure 9, it shows the variation of MSE with parameters.

In Figures 9 (a) and (b), when the dimension of the input matrix is 5, the number of hidden layer units is 40 and 80, respectively, and the dropout action intensity coefficient is 0.2. When the maximum iteration was 300, LSTM deep learning framework had high prediction accuracy. When the dimension was too large, training involved a lot of repetitive work and can also reduce learning efficiency. When the intensity of over-fittingwas too high, it can cause strong sparsity in the hidden layer, which greatly reduced the generalization ability of the LSTM deep learning framework. In Figure 9 (c), when the number of units in the first layer was set to 40, the training time took 47 seconds, and when the number was set to 200, the MSE showed multiple orders of magnitude

TABLE 1. Three different data characteristics of seismic wave displacement database.

Stats	The El-centro Wave	Tianjin Wave	Artificial wave
Database code	A	B	C
Maximum acceleration (cm/s^2)	341.7	196.3	161.6
Duration (s)	30	30	30
Sampling interval (s)	0.02	0.02	0.02
Database size (PCS)	1500	1500	1500

growth, with a training time of up to 276 seconds. Compared to increasing or decreasing hidden layers, adjusting the number of nodes in the hidden layer was simpler and had higher accuracy. However, having too many nodes in the same layer can cause non convergence and local minimization of the network. If there was too little, it resulted in insufficient weight combination. From Figure 9 (d), it can be seen that when using the A-library to build a network framework for 1000 iterations, the MSE increased by 59.3% compared to the optimal value of 300 iterations, and the training time was 183 seconds, an increase of 3.9 times. This indicated that the maximum number of iterations had a significant impact on MSE and runtime, with poor regularity, and not necessarily the more iterations the better. Using the LSTM structural response prediction model, the data from libraries A, B, and C were learnt and predicted, as shown in Figure 10, for comparison of response prediction results.

From Figure 10, it can be seen that the predicted relative difference for the C database data was the smallest, with an interval of [−0.034, 0.028] cm and a mean of −0.0053cm. The prediction error for database B data was the largest, with an interval of [−0.122, 0.160] cm and a mean of 0.015cm. Finally, the MSE of the LSTM prediction framework for E1-centro wave, Tianjin wave, and artificial wave at a total of 1500 data points in 30 seconds was 0.00182, 0.00472, and 0.00223, respectively. The LSTM prediction model had good stability, and the error distribution in earthquake response prediction was relatively concentrated, with good prediction results. The most widely used shallow learning BP neural network and RBF neural network were selected for performance comparison. As shown in Figure 11, the comparison results of the top-level control force time histories of three neural networks are presented.

In Figures 11 (a), (b), and (c), under the same iteration number, the LSTM neural network had the best predictive performance, with the highest degree of overlap with the original data at the extreme. Both RBF and BP neural networks exhibited local optima and over-fitting in their predictions, with BP having the worst performance. The maximum prediction difference among larger extreme points was 23.27%, which occured at 14.33 seconds. As shown in Figure 12 (d), the MSE of LSTM network, RBF network, and BP neural network were 3.30×10.4, 2.19×10.3, 5.53×10.3,

TABLE 2. Benchmark model parameter.

Number of floors	Quality/10^6 kg	Stiffness/ 10^3 kN/m	Storey height/m
1	1.12	862.06	5.93
1~5	1.10	862.06	3.95
6~11	1.10	554.16	3.95
12~14	1.10	453.50	3.95
15~17	1.10	291.22	3.95
18~19	1.10	256.45	3.95
20	1.10	171.69	3.95

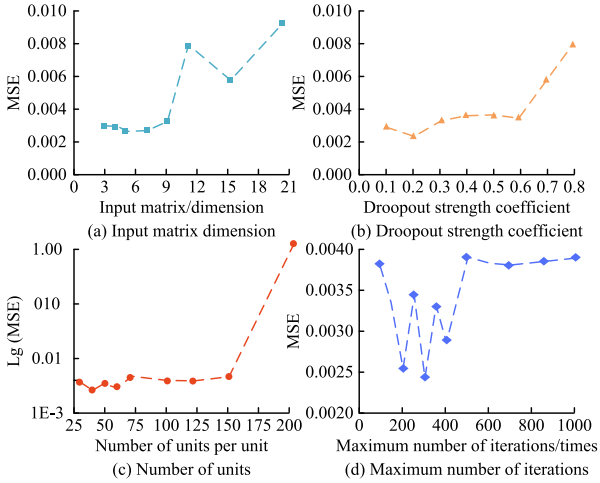

FIGURE 9. Changes of MSE with parameters.

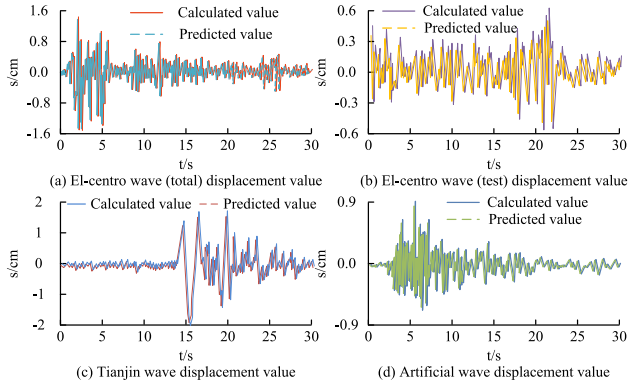

FIGURE 10. Comparison of response prediction results.

respectively. This indicated that the LSTM network had the smallest prediction error value and the best learning and prediction performance. Figure 12 shows the peak response of each floor L in both uncontrolled and controlled states when El-centro waves acted on the Benchmark model.

According to Figure 12, the control effectiveness of the three controllers (LSTM, RBF, BP) on the top displacement decreased from 38.6 mm (no control) to 18.4 mm, 20.7 mm, and 21.6 mm, respectively. The control rates were 52.1%, 46.2%, and 43.8%. The control effectiveness on velocity

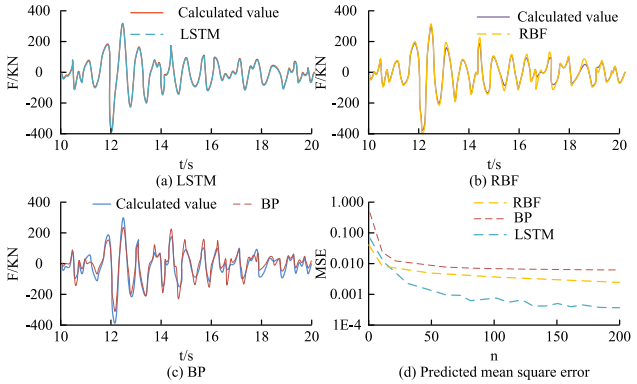

FIGURE 11. Top-level control time history comparison.

decreased from 0.36 m/s (no control) to 0.17 m/s, 0.20 m/s, and 0.21 m/s, respectively, with control rates of 51.3%, 43.1%, and 40.4%. The control effectiveness on acceleration decreased from 4.72 m/s2 (no control) to 2.46 m/s2, 3.11 m/s2, and 3.03 m/s2, respectively, with control rates of 47.7%, 33.9%, and 35.6%. The LSTM controller achieved a maximum damping ratio of 65.0% for the acceleration of the top floor, indicating its superior control effectiveness on the Benchmark model's acceleration. The robustness of the LSTM intelligent controller was studied by simulating stiffness degradation phenomena caused by seismic actions through reducing the stiffness matrix values of the Benchmark model. Table 3 shows the control effectiveness on the top displacement $a_{\max}$ under various stiffness degradation conditions.

From Table 3, it can be seen that when the degradation degree of stiffness in each layer of the Benchmark model was in the range of 10.2% −20.5%, the LSTM control effect was the best, and it remained above 39.8%. The shock-absorbing rate of the shallow learning controller for the top level acceleration was reduced to 29.56%, and there was a significant difference in shock-absorbing rate. This indicated that the LSTM robust performance was superior. The 20-layer Benchmark model proposed by ASCE was selected as a simulation example, with relevant structural parameters [27]. By using different partitioning methods, the LSTM intelligent controllers applied to the Benchmark model were designed into various decentralized control forms, as shown in Table 4.

Based on the GA-LSTM hyperparameter optimization method, a GA algorithm program in Matlab was written to optimizeLSTM sub controller's initial learning rate. The evolutionary algebra was set to 80 times, the crossover probability was set to 0.1, the population size to 8, and the mutation probability to 0.01. Figure 13 shows the population evolution curves of LSTM sub controllers under four operating conditions.

According to Figure 13, after optimization with the GA algorithm, the optimal initial learning rates for four scenarios were 0.006, 0.01, 0.006, and 0.04, respectively. The optimal fitness after 80 iterations corresponded to the LSTM

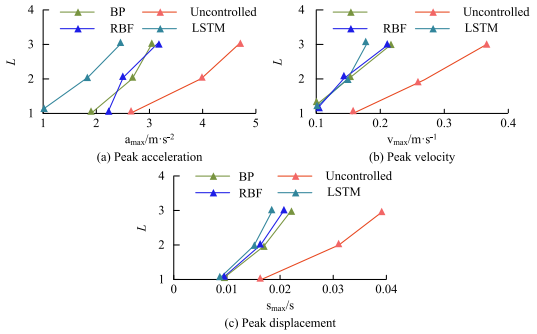

FIGURE 12. Peak response of each layer under E1-centro.

TABLE 3. Control effect of top layer amax under various stiffness degradation conditions.

Controller	Stiffness degradation ratio	a_{max} (m/s^2)	Damping ratio(%)
Uncontrolled	-10%	4.235	/
	-15%	4.465	/
	-20%	2.566	/
LSTM	-10%	2.493	41.12
	-15%	2.602	41.71
	-20%	2.706	40.71
RBF	-10%	2.536	40.11
	-15%	2.778	37.75
	-20%	2.939	35.62
BP	-10%	2.983	29.54
	-15%	2.958	33.74
	-20%	2.955	35.27

TABLE 4. Distribution of subsystems in each disperse operating condition.

Working condition	Decentralized form of control	Network structure
Condition 1	Fully decentralized -20 subsystems	4×30×1
Condition 2	Partially independent decentralized -4 subsystems	16×100×5
Condition 3	Chain topology overlapping decentralized -5 subsystems	16×100×5
		13×100×4
Condition 4	Chain topology overlapping decentralized -6 subsystems	19×100×6
		16×100×5

controller's loss function values, which were 8.3×10.5, 2.3×10.4, 2.2×10.4, and 3.0×10.4, respectively, achieving good prediction results. Compared to the commonly used trial-and-error method, this algorithm exhibited higher computational efficiency and accuracy. To further investigate the algorithm's impact on the structural response of the building, the reference paper provided evaluation indicators $EV_{\max}^{xy}$ for the Benchmark model's time history. $EV_{\max}^{xy}$ superscripts indicate displacement and acceleration, respectively, while El-centro wave and Wenchuan wave are represented by subscripts [28]. Smaller indicator values indicate better process control effectiveness. For the El-centro wave, the LQR centralized control had $EV_{\max}^{11}$, $EV_{\max}^{21}$ values of 0.5003 and 0.5934, while for the Wenchuan wave, it had $EV_{\max}^{12}$, $EV_{\max}^{22}$ values of 0.4413 and

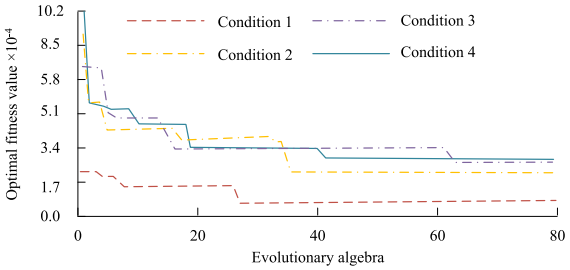

FIGURE 13. Population evolution curves of LSTM sub-controllers under four working conditions.

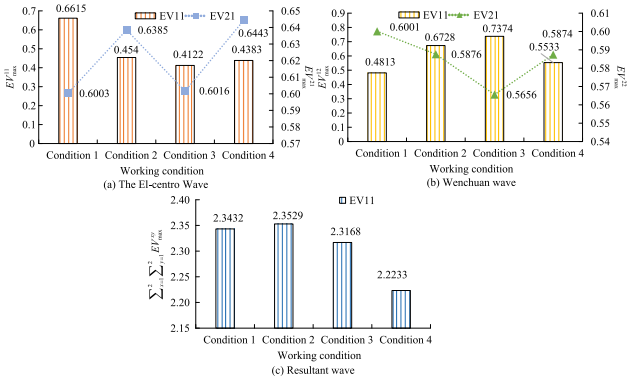

FIGURE 14. Time history evaluation indexes under different seismic excitation.

0.6209, and $EV_{\max}^{12}$, $EV_{\max}^{22}$ value of 2.1559. Figure 14 illustrates the time history evaluation indicators under different seismic excitations.

In Figure 14, GA-LSTM decentralized control with different structural forms had a good seismic reduction effect on the time-history response. GA-LSTM decentralized control had good generalization and self-learning capabilities. The evaluation indicators of condition 1-4 were reduced by 8.6%, 9.0%, 7.3%, and 6.6% compared to LQR centralized control, respectively, indicating that the time history control effect of condition 4 was closer to LQR centralized control. The time history evaluation index EV_{20}^{21} value of LQR algorithm under non-interference working conditions was 0.5119. Figure 15 shows the acceleration time history evaluation index of the 20th layer for GA-LSTM discrete control system under Gaussian white noise disturbance.

From Figure 15, it can be seen that the GA-LSTM decentralized controller designed by the research institute had good fault-tolerant performance when each sensor was subjected to different amplitude noise interference. Under the action of 10% amplitude noise, the acceleration peak of the 20th layer under four working conditions increased by 11.6%, 8.8%, 0.49%, and 1.7% compared to the original acceleration peak. As the amplitude of noise increased, the peak acceleration remained almost unchanged. Like 40% amplitude Gaussian white noise, the time history evaluation indicators EV_{20}^{21} for conditions 1-2 to 4-2 increased by 16.8%, 15.7%, 11.4%, and

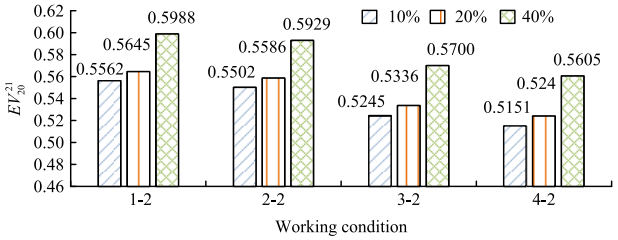

FIGURE 15. Time history evaluation indexes of Layer 20 of Benchmark model under different noise effects.

9.3%, respectively. Among them, the time history response changed the most during the 20-30s period.

V. CONCLUSION

Earthquakes have a serious impact on the normal use of buildings during their service life. In order to improve the vibration control of building structures, a high-rise building vibration intelligent control method combining genetic algorithm and LSTM has been proposed. For the 20 layer Benchmark model, LSTM centralized controllers fused with CNN hierarchical feature learning and GA-LSTM decentralized controllers with various structural forms are designed. Results showed that when the dimension of the input matrix was 5, the number of hidden layer units was 40 and 80, respectively, and the dropout action intensity coefficient was 0.2. When iteration was 300, the LSTM deep learning framework had high prediction accuracy. The relative difference in prediction for C database data was the smallest, with an interval of $[-0.034, 0.028]$ cm and a mean of -0.0053cm. The prediction error for database B data was the largest, with an interval of $[-0.122, 0.160]$ cm and a mean of 0.015cm. Finally, the MSE of the LSTM prediction framework for E1-centro wave, Tianjin wave, and artificial wave at a total of 1500 data points in 30 seconds was calculated to be 0.00182, 0.00472, and 0.00223, respectively. This indicated that the LSTM prediction model had good stability, and the error distribution in earthquake response prediction was relatively concentrated, with good prediction results. The MSE of LSTM network, RBF network, and BP neural network was 3.30×10.4, 2.19×10.3, 5.53×10.3, respectively. LSTM network had the smallest prediction error value and the best learning and prediction performance. The maximum damping rate of the LSTM controller was 65.0% of the first layer acceleration, indicating that the controller had the best control effect on the acceleration of the Benchmark model. When the degradation degree of stiffness in each layer of the Benchmark model was in the range of 10.2% -20.5%, the control effect of LSTM was the best, and it remained above 39.8%. After optimization by GA algorithm, the optimal fitness of 80 iterations was the LSTM controller loss function value, which was 8.3×10.5, 2.3×10.4, 2.2×10.4, 3.0×10.4, respectively, achieving good prediction results. Compared with the commonly used trial and error method, this algorithm had higher computational efficiency and accuracy. GA-LSTM decentralized control with different structural forms had a good seismic reduction effect on Benchmark model's time-history response. Although research has achieved good results, many hyperparameter optimization problems for LSTM intelligent controllers still need further improvement. In the future, we will also attempt to combine LSTM with other algorithms to improve the optimization effect of its hyperparameters.

REFERENCES

[1] E. Teymouri, A. J. Moradloo, and S. Abbasi, "Seismic analysis of steel tanks subjected to transitional-rotational components of earthquakes," *J. Earthq. Eng.*, vol. 27, no. 11, pp. 3153–3179, Sep. 2022, doi: 10.1080/13632469.2022.2124558.

[2] J. Liu, J. Liu, L. Fan, L. Yi, H. Song, and Q. Zeng, "Intelligent building load scheduling based on multi-objective multi-verse algorithm," *Energy Power Eng.*, vol. 13, no. 4, pp. 19–29, Apr. 2021, doi: 10.4236/epe.2021.134B003.

[3] V. M. Alexeev, L. A. Baranov, M. A. Kulagin, and V. G. Sidorenko, "Building architecture of intelligent control system for urban rail transit system," *World Transp. Transp.*, vol. 19, no. 1, pp. 18–46, Sep. 2021, doi: 10.30932/1992-3252-2021-19-1-18-46.

[4] Q. An, R. Tang, H. Su, J. Zhang, and X. Li, "Robust configuration and intelligent MPPT control for building integrated photovoltaic system based on extreme learning machine," *J. Intell. Fuzzy Syst.*, vol. 40, no. 6, pp. 12283–12300, Jun. 2021, doi: 10.3233/JIFS-210424.

[5] N. Shakeel, P. Teradata, and S. Shakeel, "Context-free word importance scores for attacking neural networks," *J. Comput. Cognit. Eng.*, vol. 1, no. 4, pp. 187–192, Sep. 2022, doi: 10.47852/bonviewJCCE2202406.

[6] Y. Song, W. He, X. He, and Z. Han, "Vibration control of a high-rise building structure: Theory and experiment," *IEEE/CAA J. Autom. Sinica*, vol. 8, no. 4, pp. 866–875, Apr. 2021, doi: 10.1109/JAS.2021.1003937.

[7] A. Hamza and N. B. Yahia, "Heavy trucks with intelligent control of active suspension based on artificial neural networks," *Proc. Inst. Mech. Eng., I, J. Syst. Control Eng.*, vol. 235, no. 6, pp. 952–969, Oct. 2021, doi: 10.1177/0959651820958516.

[8] M. Ma, L. Xu, L. Du, Z. Wu, and X. Tan, "Prediction of building vibration induced by metro trains running in a curved tunnel," *J. Vib. Control*, vol. 27, nos. 5–6, pp. 515–528, May 2020, doi: 10.1177/1077546320930910.

[9] T. Konar and A. Ghosh, "Development of a novel tuned liquid damper with floating base for converting deep tanks into effective vibration control devices," *Adv. Struct. Eng.*, vol. 24, no. 2, pp. 401–407, Jan. 2021, doi: 10.1177/1369433220953539.

[10] L. Fali, K. Zizouni, A. Saidi, T. Ghomri, I. K. Bousserhane, and M. Djermane, "Structural vibration control in excited structures: History and prospects," *J. Vibrat. Eng. Technol.*, vol. 11, no. 3, pp. 1287–1308, Apr. 2023, doi: 10.1007/s42417-022-00641-6.

[11] M. U. Saeed, Z. Sun, and S. Elias, "Research developments in adaptive intelligent vibration control of smart civil structures," *J. Low Freq. Noise, Vibrat. Act. Control*, vol. 41, no. 1, pp. 292–329, Mar. 2022, doi: 10.1177/14613484211032758.

[12] S. Elias, S. Djerouni, D. D. Domenico, and M. Abdeddaim, "Seismic response control of building structures under pulse-type ground motions by active vibration controller," *J. Low Freq. Noise Vib. Act. Control*, vol. 42, no. 1, pp. 345–367, Sep. 2022, doi: 10.1177/14613484221130192.

[13] H. Gao, J. Hu, Y. Qi, and C. Sun, "Adaptive vibration control of a flexible structure based on hybrid learning controlled active mass damping," *J. Franklin Inst.*, vol. 359, no. 12, pp. 5935–5959, Aug. 2022, doi: 10.1016/j.jfranklin.2022.06.017.

[14] C. Liu, Y. Zhang, J. Sun, Z. Cui, and K. Wang, "Stacked bidirectional LSTM RNN to evaluate the remaining useful life of supercapacitor," *Int. J. Energy Res.*, vol. 46, no. 3, pp. 3034–3043, Mar. 2022, doi: 10.1002/er.7360.

[15] L. Xiao, F. Wei, Y. Zhou, G. J. Anderson, D. M. Frazer, Y. C. Lim, T. Liu, and Y. Xiao, "Dihydrolipoic acid–gold nanoclusters regulate microglial polarization and have the potential to alter neurogenesis," *Nano Lett.*, vol. 20, no. 1, pp. 478–495, Jan. 2020, doi: 10.1021/acs.nanolett.9b04216.

[16] M. Tang, X. He, X. Yao, J. Wen, M. Bao, and L. Li, "Cyclic biaxial tensile strain enhances osteogenic differentiation in rat bone marrow-derived mesenchymal stem cells via activating ERα-Wnt3a/β-catenin pathway," *Biocell*, vol. 46, no. 6, pp. 1465–1472, 2022, doi: 10.32604/biocell.2022.018967.

[17] C. Liu, L. Cheng, L.-Y. Cui, P. Hou, B. Qian, and R.-C. Zeng, "Robust damage warning and healing tracing strategy for anticorrosion coatings on magnesium alloy AZ31 enabled by polydopamine fluorophores," *J. Mater. Sci. Technol.*, vol. 152, pp. 169–180, Jul. 2023, doi: 10.1016/j.jmst.2022.12.043.

[18] S. Veerasingam, M. Ranjani, R. Venkatachalapathy, A. Bagaev, V. Mukhanov, D. Litvinyuk, M. Mugilarasan, K. Gurumoorthi, L. Guganathan, V. M. Aboobacker, and P. Vethamony, "Contributions of Fourier transform infrared spectroscopy in microplastic pollution research: A review," *Crit. Rev. Environ. Sci. Technol.*, vol. 51, no. 22, pp. 2681–2743, Aug. 2020, doi: 10.1080/10643389.2020.1807450.

[19] T. Liu, J. Wang, X. Huang, Y. Lu, and J. Bao, "3DSMDA-Net: An improved 3DCNN with separable structure and multi-dimensional attention for welding status recognition," *J. Manuf. Syst.*, vol. 62, pp. 811–822, Jan. 2022, doi: 10.1016/j.jmsy.2021.01.017.

[20] J. Wang, T. Jiang, Z. Cui, and Z. Cao, "Filter pruning with a feature map entropy importance criterion for convolution neural networks compressing," *Neurocomputing*, vol. 461, pp. 41–54, Oct. 2021, doi: 10.1016/j.neucom.2021.07.034.

[21] G. A. S. Thomas, Y. H. Robinson, E. G. Julie, V. Shanmuganathan, S. Rho, and Y. Nam, "Intelligent prediction approach for diabetic retinopathy using deep learning based convolutional neural networks algorithm by means of retina photographs," *Comput., Mater. Continua*, vol. 66, no. 2, pp. 1613–1629, 2021, doi: 10.32604/cmc.2020.013443.

[22] G. H. Meftahi, Z. Bahari, A. Z. Mahmoudabadi, M. Iman, and Z. Jangravi, "Applications of western blot technique: From bench to bedside," *Biochem. Mol. Biol. Educ.*, vol. 49, no. 4, pp. 509–517, Apr. 2021, doi: 10.1002/bmb.21516.

[23] K. Wang, C. Ma, Y. Qiao, X. Lu, W. Hao, and S. Dong, "A hybrid deep learning model with 1DCNN-LSTM-attention networks for short-term traffic flow prediction," *Phys. A, Stat. Mech. Appl.*, vol. 583, Dec. 2021, Art. no. 126293, doi: 10.1016/j.physa.2021.126293.

[24] S. Pan, K. Yan, H. Yang, C. Jiang, and Z. Qin, "A sparse spike deconvolution method based on recurrent neural network like improved iterative shrinkage thresholding algorithm," *Geophys. Prospecting Petroleum*, vol. 58, no. 4, pp. 533–540, Apr. 2022, doi: 10.3969/j.issn.1000-1441.2019.04.007.

[25] X. Xi, M. Chen, S. Xia, and R. Lu, "Drug loading techniques for exosome-based drug delivery systems," *Pharmazie*, vol. 76, nos. 2–3, pp. 61–67, Feb. 2021, doi: 10.1691/ph.2021.0128.

[26] N. Patil, R. Ganeriwala, J. M. Solberg, N. E. Hodge, and R. M. Ferencz, "Benchmark multi-layer simulations for residual stresses and deformation in small additively manufactured metal parts," *Additive Manuf.*, vol. 45, Sep. 2021, Art. no. 102015, doi: 10.1016/j.addma.2021.102015.

[27] M. J. Khosraviani, O. Bahar, and S. H. Ghasemi, "Damage detection using both energy and displacement damage index on the ASCE benchmark problem," *Struct. Eng. Mech.*, vol. 77, no. 2, pp. 151–165, Sep. 2020, doi: 10.12989/sem.2021.77.2.151.

[28] A. Nazir, "Efficient online portfolio simulation using dynamic moving average model and benchmark index," *Int. J. Model., Simul., Sci. Comput.*, vol. 13, no. 3, pp. 161–186, Jun. 2022, doi: 10.1142/S1793962322500180.

JIJUN ZHANG received the B.E. degree in art education from Shaanxi Normal University, in 1997, and the M.E. degree in art design from the Xi'an Academy of Fine Art, in 2005. He is currently a Professor with the Department of Environment Design, School of Art and Design, XUT. His research interests include exhibition design and architecture design.

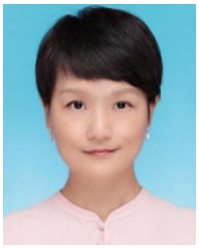

YANMIN XUE received the B.E. degree in mechanic design and manufacturing, the M.E. degree in mechanic design theory, and the Doctor (Dr.) degree in mechanic engineering from the Xi'an University of Technology, in 1996, 2002, and 2009, respectively. She is currently a Professor with the Department of Industrial Design, School of Art and Design. Her research interests include ergonomics and industrial design.